Methods & Supplementary information from J. Mark Kim et al.

A. LIST OF PLASMIDS AND STRAINS

Table A1. List of Plasmids

Plasmid	Source	Antibiotic Marker	Description
pMK4	This work	Kan	Empty vector with YFP (Venus NB)
pMK7	This work	Amp	Empty vector with CFP (SCFP3A)
pMK4-FlgA	This work	Kan	Plasmid containing flgA promoter fused to YFP (Venus NB)
pMK4-FlgB	This work	Kan	Plasmid containing flgB promoter fused to YFP (Venus NB)
pMK4-FlhB	This work	Kan	Plasmid containing flhB promoter fused to YFP (Venus NB)
pMK4-FliA	This work	Kan	Plasmid containing fliA promoter fused to YFP (Venus NB)
pMK4-FliD	This work	Kan	Plasmid containing fliD promoter fused to YFP (Venus NB)
pMK4-FliE	This work	Kan	Plasmid containing fliE promoter fused to YFP (Venus NB)
pMK4-FliF	This work	Kan	Plasmid containing fliF promoter fused to YFP (Venus NB)
pMK4-FliL	This work	Kan	Plasmid containing fliL promoter fused to YFP (Venus NB)
pMK4-FlgK	This work	Kan	Plasmid containing flgK promoter fused to YFP (Venus NB)
pMK4-FlgM	This work	Kan	Plasmid containing flgM promoter fused to YFP (Venus NB)
pMK4-FliC	This work	Kan	Plasmid containing fliC promoter fused to YFP (Venus NB)
pMK4-MotA	This work	Kan	Plasmid containing motA promoter fused to YFP (Venus NB)
pMK4-Tar	This work	Kan	Plasmid containing tar promoter fused to YFP (Venus NB)
pMK7-FliF	This work	Amp	Plasmid containing fliF promoter fused to CFP (SCFP3A)
pMK7-FliC	This work	Amp	Plasmid containing fliC promoter fused to CFP (SCFP3A)
pPro1-YFP	This work	Gent	Plasmid containing Pro1 promoter fused to YFP (Venus NB)
pPro2-YFP	This work	Gent	Plasmid containing Pro2 promoter fused to YFP (Venus NB)
pPro4-YFP	This work	Gent	Plasmid containing Pro4 promoter fused to YFP (Venus NB)
pPro5-YFP	This work	Gent	Plasmid containing Pro5 promoter fused to YFP (Venus NB)

Plasmid	Source	Antibiotic Marker	Description
pProB-YFP	This work	Gent	Plasmid containing ProB promoter fused to YFP (Venus NB)
pSIM5	Gift of D. Court	Cm	Helper plasmid encoding red recombinase proteins
pCP20	CGSC	Amp, Cm	Helper plasmid encoding FLP recombinase

Table A2. List of Strains

Strain	Source	Description
MG1655 (CGSC 6300)	CGSC	Background Strain
MG1655+IS5	This work	See below
MGR	This work	MG1655 IntS::ZeoR-P_{RNA1}-mCherry
MGR-E98K	This work	MGR *motA(E98K)*
MGR-E98K FliF FlhD ("E98KFD")	This work	MGR-E98K galK::AmpR-P_{fliF}-CFP flhDC-YFP (see below)
MGR-E98K FliF FlgA	This work	MGR-E98K galK::AmpR-P_{fliF}-CFP attB::KmR-P_{flgA}-YFP
MGR-E98K FliF FlgB	This work	MGR-E98K galK::AmpR-P_{fliF}-CFP attB::KmR-P_{flgB}-YFP
MGR-E98K FliF FlhB	This work	MGR-E98K galK::AmpR-P_{fliF}-CFP attB::KmR-P_{flhB}-YFP
MGR-E98K FliF FliA	This work	MGR-E98K galK::AmpR-P_{fliF}-CFP attB::KmR-P_{fliA}-YFP
MGR-E98K FliF FliD	This work	MGR-E98K galK::AmpR-P_{fliF}-CFP attB::KmR-P_{fliD}-YFP
MGR-E98K FliF FliE	This work	MGR-E98K galK::AmpR-P_{fliF}-CFP attB::KmR-P_{fliE}-YFP
MGR-E98K FliF FliF	This work	MGR-E98K galK::AmpR-P_{fliF}-CFP attB::KmR-P_{fliF}-YFP
MGR-E98K FliF FliL	This work	MGR-E98K galK::AmpR-P_{fliF}-CFP attB::KmR-P_{fliL}-YFP
MGR-E98K FliF FliC ("E98KFC")	This work	MGR-E98K galK::AmpR-P_{fliF}-CFP attB::KmR-P_{fliC}-YFP
MGR-E98K FliC FlgK	This work	MGR-E98K galK::AmpR-P_{fliC}-CFP attB::KmR-P_{flgK}-YFP
MGR-E98K FliC FlgM	This work	MGR-E98K galK::AmpR-P_{fliC}-CFP attB::KmR-P_{flgM}-YFP
MGR-E98K FliC FliC	This work	MGR-E98K galK::AmpR-P_{fliC}-CFP attB::KmR-P_{fliC}-YFP
MGR-E98K FliC MotA	This work	MGR-E98K galK::AmpR-P_{fliC}-CFP attB::KmR-P_{motA}-YFP

Strain	Source	Description
MGR-E98K FliC Tar	This work	MGR-E98K galK::AmpR-P_{fliC}-CFP attB::KmR-P_{tar}-YFP
E98KFD Pro1	This work	MGR-E98K galK::AmpR-P_{fliF}-CFP flhDC-YFP P_{flhD}::GentR-Pro1
E98KFD Pro2	This work	MGR-E98K galK::AmpR-P_{fliF}-CFP flhDC-YFP P_{flhD}::GentR-Pro2
E98KFD Pro4	This work	MGR-E98K galK::AmpR-P_{fliF}-CFP flhDC-YFP P_{flhD}::GentR-Pro4
E98KFD Pro5	This work	MGR-E98K galK::AmpR-P_{fliF}-CFP flhDC-YFP P_{flhD}::GentR-Pro5
E98KFD ProB	This work	MGR-E98K galK::AmpR-P_{fliF}-CFP flhDC-YFP P_{flhD}::GentR-ProB
E98KFD ΔydiV	This work	MGR-E98K galK::AmpR-P_{fliF}-CFP flhDC-YFP ydiV::FRT
E98KFC Pro4 ΔflgM	This work	MGR-E98K galK::AmpR-P_{fliF}-CFP flhDC-YFP P_{flhD}::GentR-Pro4 flgM::FRT
E98KFD Pro1 ΔydiV	This work	MGR-E98K galK::AmpR-P_{fliF}-CFP flhDC-YFP P_{flhD}::GentR-Pro1 ydiV::FRT
E98KFD Pro2 ΔydiV	This work	MGR-E98K galK::AmpR-P_{fliF}-CFP flhDC-YFP P_{flhD}::GentR-Pro2 ydiV::FRT
E98KFD Pro4 ΔydiV	This work	MGR-E98K galK::AmpR-P_{fliF}-CFP flhDC-YFP P_{flhD}::GentR-Pro4 ydiV::FRT
E98KFD Pro5 ΔydiV	This work	MGR-E98K galK::AmpR-P_{fliF}-CFP flhDC-YFP P_{flhD}::GentR-Pro5 ydiV::FRT
E98KFD ProB ΔydiV	This work	MGR-E98K galK::AmpR-P_{fliF}-CFP flhDC-YFP P_{flhD}::GentR-ProB ydiV::FRT
E98KFC+IS5	This work	MGR-E98K+IS5 galK::AmpR-P_{fliF}-CFP attB::KmR-P_{fliC}-YFP

B. STRAIN CONSTRUCTION

1) Background Strain

The background strain for this work was MG1655 (Coli Genetic Stock Center (CGSC) #6300). Two stocks of MG1655 are commonly available: MG1655 (seq) (CGSC #7740) which derives from the subculture used by the Blattner lab for the complete genomic sequencing of *E. coli* harbors an IS1 element in the regulatory region of FlhDC (1). By contrast, CGSC #6300, the original isolate of MG1655 submitted by the Blattner lab, does not have this insertion element sequence. For a discussion of the impact of this insertion element, see the section below "Impact of Insertion Element Mutation on Flagellar Transcription".

2) Chromosomal Engineering

Strains used in this study were constructed using red recombination (2). Parental strains were transformed with the helper plasmid pSIM5 and red recombination was performed using standard protocols (3). During strain construction, cells were grown at 30°C to ensure maintenance of pSIM5, which has a temperature sensitive origin. All strains were cured of the helper plasmid prior to the experiment.

3) "Scarless" Chromosomal Engineering

To generate point-mutations or insert sequences without selective markers, we used a "scarless" chromosomal engineering technique—i.e. a genome editing strategy that eliminates extraneous sequences such as antibiotic resistance cassettes(4). We modified a dual selection/counter-selection cassette in pKD45 (5) consisting of a kanamycin resistance marker and a toxin ccdB driven by a rhamnose inducible promoter (P_{RhaB}). This original cassette required counter-selection to be done on minimal M9 plates containing rhamnose because presence of other carbon sources allowed cells to avoid activation of the rhamnose promoter and escape counter selection. Cell growth was extremely slow on these plates, requiring almost two full days of incubation before colonies became visible. To overcome this limitation, we replaced the rhamnose inducible promoter with the arabinose inducible P_{araB} using standard molecular biology techniques and isothermal assembly (6) using the NEB HiFi DNA Assembly Master Mix (New England Biolabs). The resulting *kmR-araBp-ccdB* ("KAC") cassette allowed for efficient counter-selection on LB plates containing 10% arabinose. We also constructed a variant of this cassette with the gentamicin resistance (*gmR-araBp-ccdB* or "GAC").

4) Insertion of Constitutive RFP Marker

For our experiments, the background strain was first engineered to constitutively express mCherry. This modification improved identification of cells in flow cytometry experiments and facilitated segmentation of cells in time-lapse experiments. An expression cassette containing (i) a Zeocin resistance marker, (ii) a RNA-I promoter from ColE1 fused to a coding sequence for mCherry and (iii) two 100 bp long flanking sequences homologous to the IntS gene was ordered from IDT as a gBlock®. This linear fragment was chromosomally inserted into the IntS locus using the chromosomal engineering techniques described above. The insertion did not affect the growth rate under our experimental conditions or flagellar promoter activity as determined by flow cytometry. The strain harboring the constitutive red marker was designated "MGR" (MG1655 "Red").

5) Point Mutation of MotA

Motile cells can swim out of the channels in the "mother machine". To prevent the loss of cells expressing flagella from the channels, we engineered the point mutant MotA(E98K) (7) directly in the chromosome using the KAC cassette described above. This point mutation prevents MotA from powering the rotation of the flagellar motor. We confirmed via flow cytometry that this point mutation did not affect flagellar gene expression. For all time-lapse studies in the mother machine, a MGR strain harboring the MotAE98K mutation (henceforth termed "E98K") was used as the background strain.

6) Construction of Transcriptional Reporters

To generate the library of transcriptional reporters, we first generated the cloning vectors pMK4 and pMK7 which were generated from pUA66 (8). In pMK4, the GFP coding sequence and ribosomal binding site (RBS) were replaced by the RBS of Gene 10 in T7 phage ("T7 RBS") and Venus NB ("VenNB") (9). In pMK7, the GFP coding sequence and RBS were replaced by the T7 RBS and SCFP3A (9). In both cases, we empirically optimized the coding sequence of VenNB and SCFP3A for high translation rate via random mutagenesis. In pMK7, the kanamycin resistance cassette and the lambda T0 terminator were also replaced with an ampicillin resistance cassette and a high efficiency terminator from the ilvGEDA regulatory region. In addition to these changes, the original restriction cloning site was replaced with a region flanked by two BsaI recognition sites to allow for insertion of promoter sequences via Golden Gate assembly (10, 11). Both pMK4 and pMK7 were constructed by assembling PCR amplified cassettes into a circular plasmid via isothermal assembly using the NEB HiFi DNA Assembly Master Mix (New England Biolabs).

For each transcriptional reporter, we amplified via PCR a region of the chromosome encompassing the flagellar promoter of interest as well as >30bp of the coding sequences flanking the promoter. This strategy was implemented in case any previously unknown regulator binding sites existed in that region. The PCR primers were designed to contain overhangs that contained BsaI sites as well as target sequences to pMK4 or pMK7 that allowed for the assembly of the PCR product with pMK4 or pMK7 via Golden Gate assembly. The Golden Gate assembly reaction was performed as previously described, using the higher efficiency protocol of cycling between 3min incubation at 37°C and 4 min incubation at 16°C for 25 cycles (10).

The transcriptional reporters were inserted into one of two chromosomal loci. The first locus was the lambda attB site in the chromosome. The second locus was the GalK. Both loci have previously been used for the insertion of chromosomal transcriptional reporters (12-14). The two sites are approximately 20kb apart, which is sufficiently far to prevent read-through transcription (this read-through is already low due to the strong rrnB T1 terminator at the end of the VenNB cassette) from interfering with the measurements. The two sites, however, are sufficiently close to each other so that variations in chromosomal copy number during replication can safely be ignored. Integration into both sites was performed by amplifying the transcriptional reporter from the plasmid template with primers each containing at least 40bp overhang homologous to the target locus. This PCR fragment was inserted chromosomally using the techniques described above.

7) Construction of Class 1 Transcriptional Reporter

Unlike other flagellar promoters, the regulatory region of the Class 1 gene FlhDC is highly complex. Moreover, evidence suggests that transcription from this promoter may be sensitive to long range interactions (1, 15). Therefore, we decided to examine transcription of Class 1 genes by directly integrating a cassette composed of the T7 RBS and VenNB into the 3' UTR of the FlhDC transcript. One complication arises from the fact that the promoter of the neighboring gene MotA resides within the FlhC coding sequence. To avoid interference from this promoter, we replaced the codons of FlhC comprising the MotA promoter with synonymous codons. Both

the synonymous mutations and the VenNB insertion was accomplished using the "scarless" technique described above. To confirm that the insertion did not significantly alter downsteam flagellar gene expression, we inserted a Class 2 reporter in this strain and compared the distribution of fluorescence with that of the Class 2 reporter in a wild-type strain (Supplementary Figure 1B).

C. GROWTH CONDITIONS

For all experiments, except where otherwise indicated,we used a modified version of the Neidhardt EZ rich media (Teknova), an optically clear rich defined media based on a MOPS buffer (16). We replaced the 0.2% glucose in the original formulation with 0.4% glycerol to prevent catabolite repression of flagellar synthesis.

For initial experiments, cells were grown at 34ºC so that the width of the cell better matches the width of our initial microfluidic device. Subsequently, we generated additional microfluidic devices with narrower channels that permitted cell growth at 30ºC which, due to the slower generation time, permitted more fields of view to be sampled in a single experiment. The pulsating dynamics were qualitatively similar at both temperatures. Regardless, for any set of experiments where we compared multiple strains (e.g. pairwise Class II and Class III measurements, wild-type vs mutant, synthetic flhDC expression), we used identical temperature and growth conditions to enable proper quantitative comparison.

D. DATA ACQUISITION AND ANALYSIS

a. Flow Cytometry

For flow cytometry experiments, an overnight culture was diluted at least 1:3000 into 500µl of fresh growth media. Cells were incubated at 30°C with shaking at 250rpm for at least 6 hours prior to measurement. At this point, the cell density was typically around or below OD=0.1.

Cells were analyzed on a BD Fortessa flow cytometer (Becton Dickinson). The side-scatter (SSC-A) profile was used to first discriminate cells from background particles. Where possible, the constitutive red fluorescence from the mCherry marker was used as a second gate. The raw flow cytometry data was imported into MATLAB 2015b (Mathworks) and analyzed via custom software.

b. Time-Lapse Experiments in the Microfluidic Device

Microfluidic Device Preparation

In our experiments, we used an epoxy replica of the "mother machine" described in Potvin-Trottier et al (17). The replica mold was a gift from Dr. Matthew Cabeen (Harvard University, now at Oklahoma Univ.). Subsequently, we generated custom SU-8 molds to build channels that better matched the typical cell width in our growth conditions. New designs for the microfluidic device were created in AutoCAD; generally, it consists of two layers, one for the cell channels and a second one for the feeding channels. The cell channels are of 1.1 µm wide and 25 µm long. The edges of the channels are smoothed out to suppress a halo that appears on the microscope once the device is mounted. It is also added an extra area that cover all the cell channels, close to the feeding channel, to avoid the halo from that side too. The feeding channels are 8.1 mm long and 100 µm wide.

Fabrication of the master mold was carried out using standard UV photolithography in a clean room environment at the Center for Nanoscale Systems (Harvard). We modified the fabrication procedure from the method described in (17) by exposing the SU-8 using a Heidelberg MLA150 Maskless Aligner (Heidelberg Instruments). The MLA150 enabled us to directly "print" our AutoCAD designs without a mask and often resulted in more accurate printing of smaller features. To print each layer, the process was the following.

1) First layer: cell channels.
   Beside the features of the channels it is necessary to include cross marks that later will be used to align the second layer with this one.

    a. Place the wafer on spinner and rinse it by spray Acetone and IPA while it is spinning.
    b. Let it dry in a hotplate at 200°C for 15 minutes.
    c. Let it cool down and place it on spinner.
    d. Pour SU-8 2002. It should cover 2/3 of the area of the wafer. It is important in this step to avoid any bubble in the resistor, since the features are very small, and they can damage them.
    e. Spin program: Step 1: 500rpm, 100rpm/sec for 10sec. Step 2: 3500 rpm, 300 rpm/sec for 60 sec.
    f. Bake it using hot plates for: 1 min at 65°C, 1 min 95°C, 1 min at 65°C again.
    g. Exposure in the MLA with a dosage of 2500 mJ/cm2.
    h. Post bake: 1 min at 65°C, 1 min 95°C, 30 seconds at 65°C.
    i. Gently immerse the wafer in PGMA for developing. Do not spin it, otherwise the features can be washed or distorted.
    j. Hard bake for 15 minutes at 150°C.
    k. Measure the height using a profilometer. The expected height is ~1.2 µm.

2) Second layer: feeding channels.
    a. Slowly pour SU-8 2010 photoresistor on the wafer covering 2/3 of its area.
    b. Spin it using the following program: Step 1: 500rpm, 100rpm/sec for 10sec. Step 2: 3000 rpm, 300 rpm/sec for 60 sec.
    c. Bake it using hot plates for: 1 min at 65°C, 2 min 95°C, 1 min at 65°C.
    d. Use swabs with PGMA to wipe-off the alignment crosses.
    e. Bake at 65°C for 1 minute.

f. Place the wafer in the MLA, and expose it with a dosage of 4500 mJ/cm^2 and defoc -2.
g. Align the crosses using the different cameras from the MLA.
h. Once it is exposed, post bake at 65°C for 1 minute, 95°C for 4 minutes and 65°C for 1 minute.
i. Immerse the wafer in a container with PGMA and shake it at slow velocity for 1 minute.
j. Rinse with IPA.
k. Hard bake at 150 for 15 minutes.
l. Measure using the profilometer. The expected height is ~11µm

To prepare a new microfluidic device out of the mold, dimethyl siloxane monomer (Sylgard 184, Dow Corning) was mixed with the curing agent at a 10:1 ratio, degassed and poured over the mold. This mixture was degassed for an additional 1 hour and cured overnight at 65°C before being removed from the mold. Individual devices were first cut from the cured PDMS. Subsequently, inlets and outlets for each flow channel ("lane") were created using a 0.75 mm biopsy punch. The device was treated with oxygen plasma in a plasma cleaner along with a 25mm×40mm No. 1.5 coverglass (VWR) for 15s at 30W and oxygen pressure 200mTorr. Following plasma treatment, the device and glass were bonded and incubated at least 1 hour at 65°C prior to use.

Cell and growth media preparation

For time-lapse experiments, we added a passivating agent Pluronic F-108 (Sigma Aldrich) at a final concentration of 0.85g/L to the growth media. *E. coli* strains were first grown overnight in media without the passivating agent. Cells were diluted the morning of the experiment 1:100 fold in fresh media, containing the passivating agent and allowed to grow to late exponential or early stationary phase. The reduced cell size at this growth phase improved the efficiency with which cells loaded in the device.

The cell culture was loaded into the inlet of the device by pipetting. The device was then centrifuged on a custom adaptor fit into a standard table-top centrifuge at 6000g for 10 mins. The inlets were connected to syringes filled with the growth media (+passivating agent) via Tygon® tubing (VWR, ID 0.02″×OD 0.06″). The flow-through was collected from the outlet via a second Tygon® tubing into an empty beaker. The growth media was first pumped at a rate of 35µl/min for at least 1 hour to allow for the inlets and outlets to be cleared. Afterwards, the flow rate was reduced to 4-5µl/min for the duration of the experiment.

Imaging Protocol

The cells were allowed to adapt to growth in the device for at least 2 additional hours before imaging. Timelapse images in initial experiments performed at 34ºC were acquired on a Nikon Eclipse Ti inverted microscope equipped with a 60× Plan Apo oil objective (numerical aperture (NA) 1.4, Nikon), an Orca R2 CCD camera (Hamamatsu), an automated xy-stage (Ludl) and a SOLA light engine LED excitation source (Lumencor). The microscope was also surrounded by a temperature controlled enclosure. The following filter sets were used for acquisition: YFP

(Semrock YFP-2427A), CFP (Semrock CFP-2432A), and RFP (Semrock mCherry-A). Automated time-lapse acquisition was controlled using custom MATLAB 2011a (Mathworks) scripts interfacing with μManager 1.4.

Timelapse images in subsequent experiments at 30ºC were acquired on acquired with a Zeiss Axiovert 200M microscope equipped with a Plan-Apochromat 40x/1.3 Oil Ph3 Objective and a CCD camera (Hamamatsu C4742-98- 24ERG). For fluorescence excitation we used an LED illumination source, SOLA SE II (Lumencor). Filters with the following specifications were used: for YFP (Ex. 500/24, Di. 520, Em.542/27), CFP (Ex. 438/24, Di. 458, Em. 483/32) and RFP (Ex. 586/20, Di. 605, Em. 647/57). All filters were from Semrock. The variation in fluorescence intensity illumination across the field-of-view was less than 10% in all channels. The microscope setup was controlled using custom software on MATLAB 2013a (Mathworks) interfacing with μManager 1.4.

Time lapse acquisition parameters

In the Nikon microscope, images were taken every 10 minutes and focal drift was corrected via the Nikon PerfectFocus system and periodically recalibrated using z-stacks on a sacrificial position. Images in the RFP (the cell segmentation marker) were acquired at full camera resolution (1344×1024 pixels) to improve segmentation while CFP and YFP images were acquired using 2×2 binning to reduce measurement noise. Short exposure times (typically 200-300ms) and low illumination intensities (<30% of maximum illumination power) were used to minimize the effects of photobleaching.

In the Zeiss microscope, automated time-lapse acquisition was controlled using custom MATLAB (Mathworks) scripts interfacing with μManager. Images were acquired every 5 minutes. Focal drift was corrected at each acquisition step via a custom autofocus routine which acquires phase contrast images at planes above and below the previously determine optimal autofocus plane and estimates the image plane with maximal contrast. Once the new focal plane was determined, images in the YFP, CFP and RFP channels were acquired at full camera resolution (1344×1024 pixels). Again, short exposure times (typically 200-300ms) and low illumination intensities (<15% of maximum illumination power) were used to minimize the effects of photobleaching.

c. Tracking Software

We developed custom software in MATLAB to analyze our timelapse movies. Using this software, we could identify and track mother cells lineages with only occasional manual supervision. The software implements the following steps:

(i) Identification of individual cells in a single frame

For each frame, individual cells were identified and segmented using custom software implementing previously described algorithms (17-19). We used the RFP fluorescence as the "reference" channel for segmentation. Parameters of the segmentation algorithm were optimized for our typical image conditions.

(ii) Correction for shift between fluorescence channels

Once the "masks" defining individual cells were determined, images from the YFP and CFP data channels were aligned to the RFP segmentation to correct for any mis-registration between the data channels. The horizontal shift between the reference RFP channel and the data channel (YFP & CFP) was computed by taking the horizontal projection of each channel and computing the cross-correlation function: the shift was estimated from the "lag" value which gives the maximum cross-correlation coefficient. Because this shift was usually small, we limited the range of lags being computed to 5 pixels. The vertical shift was similarly computed using a cross-correlation analysis of the vertical projections of each fluorescence channel.

(iii) Tracking of the mother cell lineage

In most cases, the cell at the bottom of the growth channel (i.e. the "mother cell") remained virtually in the same position from frame-to-frame. Thus, the mother cell lineage could be easily identified by following cells closest to the "mother cell" in the previous frame. In some cases, there was a small drift in the field-of-view over the course of the experiment. However, because this drift was relatively small, it could easily be corrected by re-aligning each frame so that the mother cell remained in the center of the field of view. Potential "cell divisions" events were first identified by sudden decreases in cell area, i.e. if a cell's area dropped to less than 60% of its current value in the next frame. Manual review revealed that most lineages were properly constructed. Occasionally, however, due to mis-segmentation, the cell area increased or decreased precipitously. A "voting mechanism" similar to the algorithm described in (20) was used to correct these errors. We note, however, that measurements of mean fluorescence are very robust to these errors because usually, erroneous over-segmentation results in two symmetric "half-cells" with the same mean fluorescence as the original full size cell.

Each lineage was tracked to the end of the experiment or until the mother cells were "lost" from the channels. For simplicity, only lineages that survived to the end of the experiment were analyzed—the inclusion of shorter lineages in select cases did not substantially alter my results. Occasionally, cells in the tracks grew filamentous or stopped growing altogether. These lineages were discarded from analysis.

(iv) Measurement of fluorescence and cell length

Once the cells corresponding to the mother cell lineage were identified in each frame, we extracted the mean fluorescence and cell length measurements. Mean fluorescence was computed by collecting the pixels of the fluorescence image that lie within the mask corresponding to the mother cell, summing those values and then dividing by the number of pixels. We computed the mean fluorescence in all three (YFP, CFP and RFP) fluorescence channels. For each mother cell, we also estimated the approximate cell length: due to the fixed orientation of the cells, the vertical distance between the top- and bottom-most pixels of the mother cell provided reasonable estimates of the cell length without requiring intensive computation.

d. Time lapse data analysis

(i) Estimation of promoter activity

The activity of a promoter driving a transcript expressing a fluorescent protein can be estimated by the amount of new fluorescent protein produced between two time points. The fluorescent

proteins used in our experiments are generally very stable and undergo negligible degradation. Under such conditions:

$$F_{total}(t) \cong F_{total}(t-1) + P(t)$$

where F_{total} is the total fluorescence of the cell and P(t) is the amount of new fluorescence produced between t-1 and t. Thus, in principle, we could estimate P from the change is total fluorescence within the cell between two frames. However, estimation of the total fluorescence is highly sensitive to exact segmentation of each individual cell. Therefore, we instead opted to use methods of promoter activity estimation based on changes in the mean fluorescence (i.e. the average pixel intensity) in the cell as previously described in (17, 21). Briefly, if the total area of the cell is A(t) and the average pixel intensity is C(t), then $F_{total} = A(t)C(t)$. It follows that $\frac{dF_{total}}{dt} = C\frac{dA}{dt} + A\frac{dC}{dt}$ which can be rearranged to give:

$$\frac{1}{A}\frac{dF_{total}}{dt} = C\frac{1}{A}\frac{dA}{dt} + \frac{dC}{dt}$$

We chose to use the left term $\frac{1}{A}\frac{dF_{total}}{dt}$, i.e. the "cell-size normalized" production rate, as a proxy for promoter activity. Because the transcriptional pulses we observed were extremely large and lasted multiple cell generations, this normalization had a negligible effect while simplifying our promoter activity estimation. Operationally, we estimated $\frac{1}{A}\frac{dA}{dt}$, i.e. the relative growth rate of the cell, by taking the log ratio of the initial and final area of the cell for each cell division. We estimated $\frac{dC}{dt}$ by smoothing our fluorescence traces with a Savitzky-Golay filter and taking the numerical derivative.

(ii) Estimation of "on" and "off" states

To estimate the duration of "on" and "off" states, we first applied a mild Savitzky-Golay filter to our promoter traces. We then defined a heuristic threshold to identify the "pulse on" and "pulse off" states for each promoter. First, using cells without any fluorophores, we estimated the background "promoter activity" of *E. coli* under our experimental conditions which arises due to autofluroescence. From this measurement, we obtained the mean and standard deviations of autofluorescence-associated background activity. We defined the mean + 2×standard deviation of this background activity as our "low detection threshold". When we applied this threshold to our Class II and Class III promoter activity traces, we discovered that this threshold was too sensitive and that we detected many small "bursts" of transcription lasting under 10 minutes. We hypothesized that those bursts might be "leaky" transcripts that occur even during inactive states. Therefore, collected all short bursts, lasting 10 minutes or less and computed the mean and standard deviation of those bursts. This process allowed us to define a second threshold as the mean + 2×standard deviation of "leaky transcript" activity. Time periods when the promoter activity was continuously above this threshold was defined as "on" periods. Similarly, "off" periods were defined as contiguous time periods with promoter values below this threshold.

(iii) Correlation analysis

Autocorrelations of promoter activity traces were computed using the *xcov* function in MATLAB. The average autocorrelation function was obtained by taking the mean

autocorrelation value for all the traces for each time lag. The Pearson correlation coefficients between two traces (or between YFP and CFP fluorescence in individual cells) was computed using the *corr* function in MATLAB. The mean correlation coefficient for each strain was obtained by averaging correlation coefficients from multiple independent lineages.

(iv) Input-output relationship between promoters across different classes

To determine the input-output relationship between Class II and Class III, we divided the Class II reporter fluorescence into 8 logarithmically-spaced bins that spanned the minimum and maximum Class II fluorescence values measured. For each bin we computed the mean input (i.e. mean Class II fluorescence) against the mean of the corresponding output (i.e. Class III promoter activity).

Similarly, to determine the input-output relationship between Class I and Class II in strains where Class I was driven by different synthetic promoters, we divided the Class I reporter fluorescence into 5 logarithmically-spaced bins that spanned the minimum and maximum Class I fluorescence values measured. For each bin we computed the mean input (i.e. mean Class I fluorescence) against the mean of the corresponding output (i.e. Class II promoter activity).

E. IMPACT OF INSERTION ELEMENT MUTATION ON FLAGELLAR TRANSCRIPTION

The heterogeneity in flagellar gene expression appears to contradict previous physiological observations that mid-exponential phase cells have on average 2-3 flagella each (22-24). However, as noted before, traditional strains used in chemotaxis studies (such as RP437 or W3110) have been shown to harbor in insertion element in the regulatory region of *flhDC* (1). The experimental strain MG1655 used here, however, has the wild-type regulatory sequence without the insertion element mutation. To determine whether the apparent difference in flagellar gene regulation might be specifically due to the insertion element mutation, we replaced the native FlhDC regulatory region with a homologous region from W3110 which carries an IS5 insertion. This "IS5" strain of MG1655 began expressing flagellin homogenously at a high level (Supplementary Figure 2). This result supports our hypothesis that the pulsing behavior may have been previously obscured in many common *E. coli* strains that harbor the insertion element.

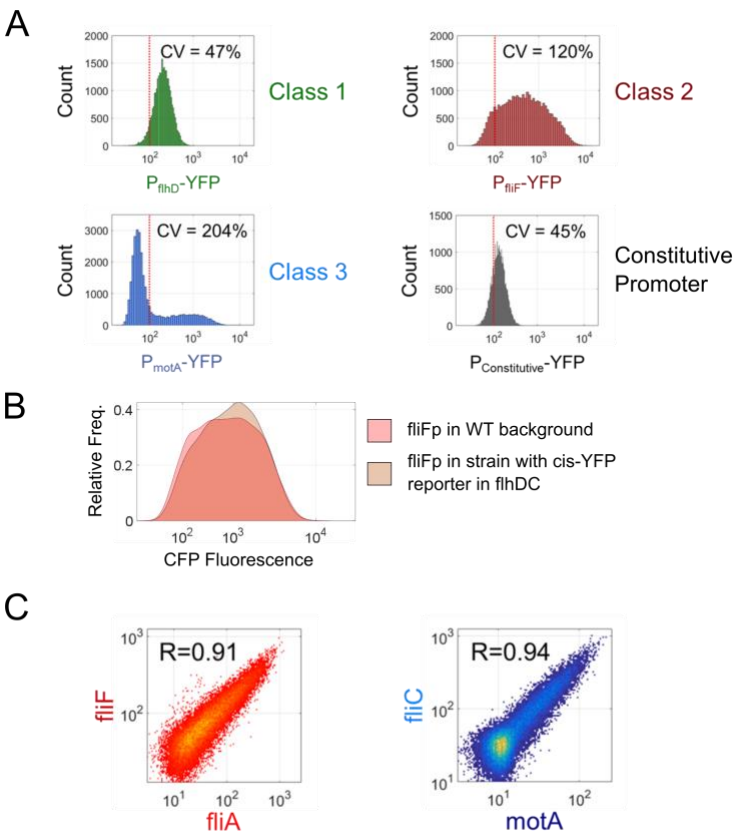

Supplementary Figure 1. (A) Typical fluorescence distribution of Class 1, 2 and 3 promoters. Shown is the fluorescence distribution of cells harboring the flhD, fliF or motA promoters fused to YFP and measured via flow cytometry. Also shown is the fluorescence distribution of a constitutive promoter (Pro4) with similar mean expression to the wild-type flhD promoter. Coefficient of variation (CV) values are for each fluorescence distribution. (B) Fluorescence distribution of CFP in strains with a Class II (fliF)-CFP reporter with (brown) and without (red) the cis-YFP reporter in FlhDC. (C) Typical distribution of fluorescence in cells harboring two Class 2 promoter reporters (left) or two Class 3 promoters (right), measured via flow cytometry. (Left) Shown is a 2D density plot of YFP and CFP fluorescence in cells harboring the fliA promoter fused to YFP and the fliF promtoer fused to CFP. (Left) Shown is a 2D density plot of YFP and CFP fluorescence in cells harboring the motA promoter fused to YFP and the fliC promtoer fused to CFP. The R value indicates the Pearson correlation coefficient.

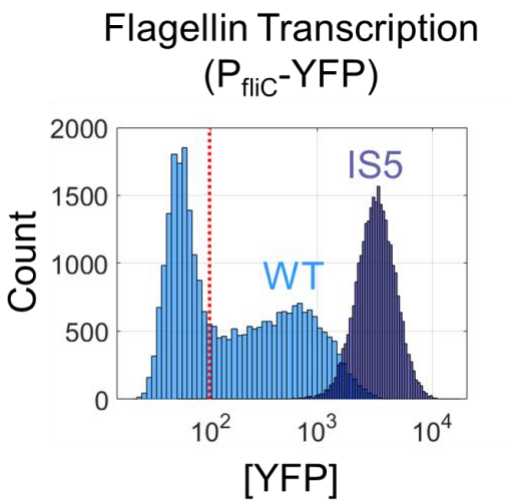

Supplementary Figure 2. Distribution of fluorescence in cells with P_{fliC}-YFP measured via flow cytometry. Wild type strains (WT, light blue) show large heterogeneity while insertion element mutants (IS5, dark blue, see SI text) express flagellin homogeneously. Dashed red line indicates 2σ threshold for cellular auto-fluorescence (measured from cells without any fluorescent reporters).

1. Barker CS, Pruss BM, & Matsumura P (2004) Increased motility of Escherichia coli by insertion sequence element integration into the regulatory region of the flhD operon. *J Bacteriol* 186(22):7529-7537.
2. Copeland NG, Jenkins NA, & Court DL (2001) Recombineering: a powerful new tool for mouse functional genomics. *Nat Rev Genet* 2(10):769-779.
3. Sharan SK, Thomason LC, Kuznetsov SG, & Court DL (2009) Recombineering: a homologous recombination-based method of genetic engineering. *Nat Protoc* 4(2):206-223.
4. Li XT, Thomason LC, Sawitzke JA, Costantino N, & Court DL (2013) Positive and negative selection using the tetA-sacB cassette: recombineering and P1 transduction in Escherichia coli. *Nucleic Acids Res* 41(22):e204.
5. Kolmsee T & Hengge R (2011) Rare codons play a positive role in the expression of the stationary phase sigma factor RpoS (sigma(S)) in Escherichia coli. *RNA Biol* 8(5):913-921.
6. Gibson DG, *et al.* (2009) Enzymatic assembly of DNA molecules up to several hundred kilobases. *Nat Methods* 6(5):343-345.
7. Morimoto YV, Nakamura S, Kami-ike N, Namba K, & Minamino T (2010) Charged residues in the cytoplasmic loop of MotA are required for stator assembly into the bacterial flagellar motor. *Mol Microbiol* 78(5):1117-1129.
8. Zaslaver A, *et al.* (2006) A comprehensive library of fluorescent transcriptional reporters for Escherichia coli. *Nat Methods* 3(8):623-628.
9. Balleza E, Kim JM, & Cluzel P (2018) Systematic characterization of maturation time of fluorescent proteins in living cells. *Nat Methods* 15(1):47-51.
10. Engler C, Kandzia R, & Marillonnet S (2008) A one pot, one step, precision cloning method with high throughput capability. *PLoS One* 3(11):e3647.
11. Engler C, Gruetzner R, Kandzia R, & Marillonnet S (2009) Golden gate shuffling: a one-pot DNA shuffling method based on type IIs restriction enzymes. *PLoS One* 4(5):e5553.
12. Datsenko KA & Wanner BL (2000) One-step inactivation of chromosomal genes in Escherichia coli K-12 using PCR products. *Proc Natl Acad Sci U S A* 97(12):6640-6645.
13. Dunlop MJ, Cox RS, 3rd, Levine JH, Murray RM, & Elowitz MB (2008) Regulatory activity revealed by dynamic correlations in gene expression noise. *Nat Genet* 40(12):1493-1498.
14. Elowitz MB, Levine AJ, Siggia ED, & Swain PS (2002) Stochastic gene expression in a single cell. *Science* 297(5584):1183-1186.
15. Lee C & Park C (2013) Mutations upregulating the flhDC operon of Escherichia coli K-12. *J Microbiol* 51(1):140-144.
16. Neidhardt FC, Bloch PL, & Smith DF (1974) Culture medium for enterobacteria. *J Bacteriol* 119(3):736-747.
17. Potvin-Trottier L, Lord ND, Vinnicombe G, & Paulsson J (2016) Synchronous long-term oscillations in a synthetic gene circuit. *Nature* 538(7626):514-517.
18. Norman TM, Lord ND, Paulsson J, & Losick R (2013) Memory and modularity in cell-fate decision making. *Nature* 503(7477):481-486.
19. Uphoff S, *et al.* (2016) Stochastic activation of a DNA damage response causes cell-to-cell mutation rate variation. *Science* 351(6277):1094-1097.
20. Yang Y, Song X, & Lindner A (2016) Time-lapse microscopy and image analysis of Escherichia coli cells in mother machines. *Methods in Microbiology* 43:49-68.
21. Levine JH, Fontes ME, Dworkin J, & Elowitz MB (2012) Pulsed feedback defers cellular differentiation. *PLoS Biol* 10(1):e1001252.
22. Makinoshima H, *et al.* (2003) Growth phase-coupled alterations in cell structure and function of Escherichia coli. *J Bacteriol* 185(4):1338-1345.

23. Tang H & Blair DF (1995) Regulated underexpression of the FliM protein of Escherichia coli and evidence for a location in the flagellar motor distinct from the MotA/MotB torque generators. *J Bacteriol* 177(12):3485-3495.
24. Turner L, Ryu WS, & Berg HC (2000) Real-time imaging of fluorescent flagellar filaments. *J Bacteriol* 182(10):2793-2801.